Microwave-assisted preparation of almond shell-based activated carbon for methylene blue adsorption

Du, Chunfeng; Yang, Hongbing; Wu, Zhansheng; Ge, Xinyu; Cravotto, Giancarlo; Ye, Bang-Ce; Kaleem, Imdad. Microwave-assisted preparation of almond shell-based activated carbon for methylene blue adsorption. GREEN PROCESSING AND SYNTHESIS. 5 (4) pp: 395-406.
DOI: 10.1515/gps-2016-0032

Microwave-assisted preparation of almond shell-based activated carbon for methylene blue adsorption

Chunfeng Du[a], Hongbing Yang[a], Zhansheng Wu [a, b*], Xinyu Ge[a], Giancarlo Cravotto[b], Bang-Ce Ye[a], Imdad Kaleem[c]

a School of Chemistry and Chemical Engineering, Shihezi University, Shihezi 832003, P.R. China

b Dipartimento di Scienza e Tecnologia del Farmaco, University of Turin, Turin 10125, Italy

c COMSATS Institute of Information Technology (CIIT), Islamabad, 45550, Pakistan.

Corresponding author: Zhansheng Wu, Shihezi University, Shihezi 832003, P.R. China.

Tel: 86993-2055015, Fax: 86993-2057270. E-mail address: wuzhans@126.com

Abstract

In this study, a novel adsorbent designated as almond shell-based activated carbon (ASAC) was synthesized from waste almond shells (AS) through exposure to microwave radiations and usage of $ZnCl_2$ as a chemical activator. The ramifications of synthetic conditions were further elaborated by response surface methodology to optimize the adsorption capacity of ASAC for methylene blue (MB) dye. The determined optimized conditions of ASAC preparation were such as: mass ($ZnCl_2$/AS) ratio of 3:1 (w/w) and microwave heating time period of 15 min at 900 W, while the maximum obtained yield of ASAC was 39.67%, with an adsorption capacity of 314.20 mg/g for MB. In addition, ASAC was characterized by N_2 adsorption-desorption measurement, scanning electron microscopy, Fourier-transform infrared spectrometry (FTIR), X-ray photoelectron spectroscopy (XPS) and point of zero charge measurement. The optimized ASAC had a Brunauer-Emmett-Teller surface area of 839.60 m^2/g and a total volume of 0.406 cm^3/g. FTIR and XPS analysis exhibited a decline in oxygen-containing groups of ASAC as compared with AS. The adsorption behavior of ASAC for MB was fitted well to the pseudo-second-order model and the Langmuir isotherm model. These findings support the economical and promising preparation of ASAC to be employed in environmental remediation.

Keywords: Activated carbon; Microwave; Almond shell; Response surface methodology; Methylene blue.

1. Introduction

In recent years, activated carbon (AC) has been widely employed in chemical industry due to its textural characteristics, high surface area, and surface adsorption properties. It has a very broad range of industrial applications such as separation/purification of liquids and gases, removal of toxic substances, catalysts and catalyst support, super capacitors, electrodes and gas storage [1]. One of the biggest challenges in commercial manufacturing of AC is to find a novel inexpensive precursor that has potential economic benefits and is available in large quantities to meet its rising demands. So far, many efforts have been made to produce AC from renewable sources and precursors from agricultural wastes such as oil palm shell [2], coconut husk [3], rambutan peel [4], edible fungi residues [5], and acorn shell [6]. Xinjiang, the largest autonomous region of China, produces a large amount of almond shells (AS) annually, and its annual output reached up to 60,000 tons in 2014 making it a significantly important agricultural waste. The utilization of such waste material like AS in the commercial production of AC would facilitate the development of a low-cost alternative precursor.

Due to heavy industrialization, there is a continuous emission of various pollutants in the environment particularly dyes which cause a serious threat to aquatic life. Methylene blue (MB) is the most commonly used substance in the dying process and has potential risks towards the environmental pollution; therefore, it was selected as a model adsorbate in this study to determine the adsorption efficiency of our novel synthetic adsorbent.

The general process of AC production requires high heat energy which is provided by two different ways such as conventional heating and microwave heating [7]. Conventional heating method is usually used in the industrial preparation of AC which demands higher activation

temperature and longer activation time, thereby leading to considerably lower yield and higher energy cost. Achawa et al. prepared the coconut shell-based activated carbon by conventional heating method by physical activation for 120 min, the result material had a surface area (S_{BET}) of only 524 m^2/g [8]. Microwaves supply energy to the carbon particles, and this energy is converted into heat within the particles themselves by dipole rotation and ionic conduction [9]. Microwave heating has been recently employed for the preparation of AC. Junior et al. synthesized a highly porous AC from macadamia nut endocarp by chemical activation with $ZnCl_2$ via microwave radiations [10]. Njoku et al. also introduced a microwave-induced activation process to prepare a high-surface area AC from rambutan peel [4]. Hesas et al. revealed AC production from oil palm shells through microwave-induced $ZnCl_2$ activation [2]. By using microwave technique, it is possible to produce activated carbon by an easy and a quick way, it has potential benefits over conventional heating such as short treatment time, low energy cost, high heating rate, selective heating, and controllable heating process [11, 12]. All recent reports have validated the use of microwave-induced activation process due to its faster activation rate and higher carbon yield. Therefore, microwave heating is considered as a viable alternative for conventional heating methods.

Response surface methodology (RSM) has a great significance in the optimization of the process conditions, analyzing the interaction between the effective process parameters, and identification of the factor settings that optimize the response [3]. The RSM method has been employed by many researchers to amplify AC production by using conventional heating methods [13]. Hence, RSM has sound applications in refined and optimized production of ACs. However, to the best of our knowledge, not a single research work is available on RSM

based optimized synthetic conditions for AS-derived ASAC production via microwave heating.

The present study designed to investigate the use of microwave-induced activation procedure to prepare highly porous almond shell-based activated carbon from AS, and its adsorption efficiency for MB. The influences of activation time, microwave power, and mass ratio on MB adsorption and yield of ASAC were thoroughly investigated. We used Box–Behnken design (BBD) to select the effects of the three main variables and RSM to optimize the synthetic conditions. In addition, scanning electron microscopy (SEM), Fourier-transform infrared spectrometry (FTIR), X-ray photoelectron spectroscopy (XPS), and other analytical techniques were used to characterize ASAC. Furthermore, the adsorption isotherms and kinetics were also elucidated. The proposed synthetic method of ASAC through microwave heating has a great potential in economical production of an excellent adsorbent having an enormous remedial effects against various industrial wastes particularly for water pollutants.

2. Materials and methods

2.1 Raw material

The AS was purchased from the local market, washed with distilled water and dried in an oven at 100 °C for 24 h to remove the moisture content. The dried AS were crushed and sieved to a uniform particle size of 100 meshes. The proximate analyses of AS were ash 1.67%, fixed carbon 29.40%, moisture 5.31% and volatilizes 63.62%. All analyses were performed in three replicates.

2.2 Preparation of ASAC

The microwave-assisted process was performed using a modified microwave oven (MM823LA6-NS, Midea) at a frequency of 2.45 GHz. The 4.0 g of mixture with different mass ratios (X_1) of $ZnCl_2$ and AS of a particle size of 100 meshes were put in a quartz tube reactor placed into microwave oven. Then the activation processes were subjected to different microwave heating times (X_2, min) and microwave radiation powers (X_3, W) under 100 cm^3/min of nitrogen flow. The resulting material was washed repeatedly with hot distilled water until the pH solution reached a value of 7.0. The obtained ASAC were dried at 80 °C for 24 h, and then stored for further analyses.

The percentage of ASAC yield was calculated using the following equation:

$$Y\ (\%) = \frac{W}{W_0} \times 100 \quad (1)$$

where W is the weight of the prepared ASAC after activation and W_0 is the weight of the raw materials before activation.

2.3 Experimental design and response surface methodology

RSM was applied to optimize the activation process as it is a useful statistical tool for modeling and analysis of multivariable. This method was chosen for fitting a quadratic surface with the fewest number of experiments. In this step, BBD method was applied in three levels in order to design the activation experiments. Table 1 shows the ranges and levels of the experimental parameters: mass ratio (X_1), activation time (X_2), and microwave power (X_3). The MB adsorption (Y_1) was taken as the process responses.

In order to study the relationship between the response variable (MB number and yield) and independent variables, the experimental data were fitted to a second-order polynomial regression model, expressed by Eq. (2)

$$Y = \beta_0 + \sum_{i=1}^{k} \beta_i \chi_i + \sum_{i=1}^{k} \beta_{ii} \chi_i^2 + \sum_{i=1}^{k} \sum_{j=i+1}^{k} \beta_{ij} \chi_i \chi_j + \varepsilon \quad (2)$$

where Y is the response variable, x_i and x_j are the independent variables, $\beta_0, \beta_i, \beta_{ii}$ and β_{ij} are the regression coefficients (β_0 is constant term, β_i is the linear effect term, β_{ii} is quadratic effect term, β_{ij} is the interaction effect term).

Design Expert software (version 8.0.6, Stat-Ease Inc., Minneapolis, USA) was used to elaborate the experimental design, evaluate the model, and estimate the subsequent regression, variance, and response surface analysis.

2.4 Characterization of ASAC

Some physical properties, textural morphology and chemical properties of ASAC were measured by renowned analytical techniques. The surface physical properties of the ASAC were characterized with Quanta Chrome Instruments Quadrasorb SI, using N_2 adsorption measurements at 77 K. The S_{BET} was calculated with the (Brunauer-Emmett-Teller) BET equation. The nitrogen volume held at the highest relative pressure ($P/P_0 = 0.95$) was used to calculate the total pore volume of the ASAC. The micropores surface area, volume, and external surface area were obtained using the t-plot method.

SEM was also employed to study the textural structure of the raw material and the adsorbent after the activation process. The morphology of AS and ASAC were characterized by SEM (JEOL, JSM-6490LV, Japan) with a secondary electron beam and an acceleration voltage of 3 kV. The samples were coated with gold to ensure that the particles have suitable conductivity after drying overnight at 80 °C under vacuum.

Chemical characterization of surface functional groups was inspected by FTIR (Magna-IR 750, Nicolet) in the scanning range of 4000–400 cm^{-1}, 10 scans were taken at a resolution of

1 cm^{-1}. The samples were mixed with KBr powder and the mixtures were pressed into pellet.

Meanwhile, the surface chemical element content at the surface of AS and ASAC was performed using XPS. The XPS analysis was conducted using AMICUS/ESCA 3400 spectrometer with Mg radiation at 240 W and 12 kV under ultrahigh vacuum. Pass energy was set as 276 and 300 eV for survey and high-resolution spectra, respectively. The XPS spectra were calibrated by taking the graphitic peak as 284.5 eV. The surface atomic concentrations were calculated from the survey spectra after correcting the relative peak areas by sensitivity factors.

The determination of point of zero charge (pH_{pzc}) was conducted by adjusting the pH of 50 mL 0.1 mol/L NaCl solution (prepared in boiled water to eliminate CO_2) to a value between 2 and 12. Approximately 0.15 g of ASAC was added and the final pH was measured after 48 h under agitation. The pH_{pzc} is the point where $pH_{initial} - pH_{final} = 0$.

2.5 Adsorption capacity

0.1 g of ASAC was put into 150 mL Erlenmeyer flask with stopper containing 50 mL of MB solution of initial concentration of 1.5 g/L at pH=6.16 for determining the adsorption capacity of ASAC for MB. The flask was vibrated at 170 rpm in a thermostated waterbath shaker at around 20 °C. After adsorption equilibrium time of 30 min, which obtained by a series of preliminary experiments, Samples were separated by filtration, the concentration of MB solution was analyzed by absorbance measurements using a double beam UV-75N at a wavelength of 665 nm. The MB uptake of ASAC, q (mg/g), was calculated by Eq. (3):

$$q = \frac{(C_0 - C_e)V}{M} \quad (3)$$

where C_0 (mg/L) and C_e (mg/L) are the initial and equilibrium concentrations of MB,

165 respectively, V (L) is the volume of solution and M (g) is the dry mass of ASAC.

166 **2.6 Adsorption kinetics**

167 The procedures of the adsorption kinetics were carried out at the initial MB concentrations
168 set as 300 and 500 mg/L at 20 °C, respectively. 0.1g ASAC were put into 150 mL conical
169 flasks with 50 mL MB solution, the samples were separated by filtering at different contacting
170 time intervals (2, 5, 10, 15, 30, 45, 60, 120 min). And the residual concentrations of MB were
171 measured and adsorption amounts of ASAC were calculated with above method.

172 To understand the adsorption dynamics of MB on ASAC in relation to time, the
173 experimental data were analyzed using the pseudo-first-order [14] and pseudo-second-order
174 [15] kinetic models. The expression of the pseudo-first-order kinetic model is given by Eq.
175 (4):

176 $$q_t = q_e(1\text{-}e^{\text{-}k1t}) \quad (4)$$

177 where q_e (mg/g) is the amount of MB adsorbed at equilibrium, k_1 (h^{-1}) is the
178 pseudo-first-order rate constant, and t (h) is the contact time. The form of the
179 pseudo-second-order kinetic model is given by Eq. (5):

180 $$q_t = \frac{q_e^2 k_2 t}{1 + q_e k_2 t} \quad (5)$$

181 where k_2 is the pseudo-second-order rate constant (g/mg min).

182 **2.7 Adsorption isotherms**

183 To analyze the validity of the adsorption data, the Langmuir and Freundlich adsorption
184 models were run as discussed below. Adsorption isotherms of activated carbon was
185 determined the adsorption amounts of different concentration (50, 200, 300, 550, 850, 910
186 and 1000 mg/L) of MB under the equilibrium adsorption time of 30 min.

The Langmuir isotherm equation [16], which is the most commonly used for monolayer adsorption on to a surface with a finite number of identical sites, was represented by the following Eq. (6):

$$q_e = \frac{q_m K_L C_e}{1 + K_L C_e} \quad (6)$$

where C_e (mg/L) is the equilibrium concentration of the MB dye, q_m (mg/g) is the maximum adsorption capacity and K_L (L/mg) is the Langmuir adsorption equilibrium constant (L/mg), which is related to the affinity of the binding sites.

The Freundlich isotherm equation [17], the most important multilayer adsorption isotherm for heterogeneous surfaces, is described by the following Eq. (7):

$$q_e = K_F C_e^{1/n} \quad (7)$$

where K_F ((mg/g)·(L/mg)$^{-1/n}$) and n are Freundlich parameters related to the adsorption capacity and adsorption intensity, respectively.

3. Results and discussion

3.1. RSM and model fit

BBD was used to elaborate correlation between the activated carbon preparation variables to the MB adsorption and yield. Seventeen experiments were performed for the RSM optimization of three parameters at three levels. The results of these experiments are presented in Table 1. Runs 13–17 at the center point were used to check the experimental error. The Q_m values for ASACs, which were prepared according to the experimental conditions, ranged from 164.82 to 314.20 mg/g, while the yield of carbon obtained ranged from 31.0% to 49.7%. For the response of MB adsorption value, the quadratic model was selected, as suggested by the software. The final empirical model in terms of coded factors for MB

adsorption value (Y_1) was shown in Eq. (8)

$$Y_1 = 203.71 + 44.81X_1 + 7.46X_2 + 18.67X_3 + 3.70X_1X_2 + 11.17X_1X_3 - 11.24X_2X_3 + 23.45X_1^2 - 13.79X_2^2 + 1.17X_3^2 \quad (8)$$

Negative signs in front of the terms indicate antagonistic effects, whereas the positive signs indicate synergistic effects. Variance was employed to justify the adequacy of the model. Variance for the quadratic model of MB adsorption is shown in Table 2, where the F-value of 9.92 and Pr > F of 0.0032 proved that the model is significant. The value of model terms Pr > F less than 0.05 indicates that the model terms are significant. The results showed that X_1, X_3 and X_1^2 are all significant model terms. These significant effects signified the importance and effectiveness of the selected independent variables for the experiments. As shown in the variance analysis, the lack-of-fit-test was non-significant, indicating that the model can be well fitted to the studied data. The 3D response surface (Fig. 1) is generally the graphical representation of the regression equation. The effect of heating time on the experimental response of Q_m values can be seen in Figs. 1a and 1c. The heating time has only a weak effect on the MB adsorption capacity. The indistinctive effect of the microwave heating time on the adsorption capacity values was also reported by Zhong et al. [18]. Fig. 1a and 1b exhibited the effect of the mass ratio on the response. The value of Q_m evidently increased with the increase in mass ratio at high microwave power levels. The use of the activating reagent in the microwave-assisted activation could promote the breaking of bonds in the precursors and elimination of some volatile species from the precursors [19]. As a result, ASACs with increased surface area and higher adsorption capacity are obtained. Our results on the effect of microwave power (Figs. 1b and 1c) demonstrated that the highest values of Q_m could be

obtained at a microwave powers over 820 W. This trend was attributed that the high microwave power could increase the temperature of the system, reduce the activation energy of the carbon–reagent reaction and promote the development of pores on the materials [20].

Fig. 1 should be put here.

3.2 Process optimization

The preparation of ASAC with adsorption efficiency toward organic compounds, such as MB dye, is the most important aspect of its potential economic feasibility and marketing. Design Expert software version 8.0.6 was used to compromise adsorption capacity while optimizing the value by selecting the highest responses from the experimental results. The optimum calculated conditions were a mass ratio of 3:1, an activation time of 15 min, and a microwave power of 900 W. Under optimal conditions, a carbon yield of 41.19% and an MB adsorption capacity of 285.69 mg/g were predicted. Meanwhile, the practical repeat experiments were carried out to justify the accuracy of the predicted results which showed the carbon yield of 39.67% and an MB adsorption capacity of 314.20 mg/g. The relative errors for the carbon yield and MB adsorption capacity between the experimental and predicted values are 3.69% and 9.07%, respectively, which indicates the sufficient accuracy of the process optimization. The present study reveals the remarkable adsorption capacity of MB onto ASAC (Table 3) as compared to previously reported adsorbents [11, 21-23].

3.3Characterization of ASAC

3.3.1 Specific surface area and pore structure of ASAC

The N_2 adsorption–desorption isotherm at 77 K is shown in Fig. 2a. The isotherm resembles a combination of type I and type II isotherms, as defined by IUPAC; this adsorption

behavior exhibits characteristics of microporous–mesoporous structures [24]. The pore size distribution of ASAC is shown in Fig. 2b. The sharpest peak is observed at a pore diameter between 0.5 and 1.0 nm, with an average pore size of 0.83 nm, which indicated the essentially microporous texture of ASAC. The specific surface area was calculated by the BET equation, which was 839.60 m^2/g. The structural characteristics of ASAC are listed in Table 4. ASAC exhibited a relatively high S_{BET} of 839.60 m^2/g and a V_T of 0.406 cm^3/g as compared to previous studies.

Fig. 2 should be put here.

3.3.2 SEM analysis of ASAC

Fig. 3 shows SEM images of AS and ASAC prepared under the optimum conditions (i.e., mass ratio of 3:1, activation time of 15 min, and microwave power of 900 W). The surface of the AS is planar, undulating and mainly consists of macropores. The number of pores of the ASAC significantly increased after the activation process. ASAC surface exhibited a well-organized, pronounced, and uniform porosity (Fig. 3b), which significantly increased its surface area, and resulted in more pores available for MB adsorption. This observation was supported by the physical parameters as summarized in Table 3, which highlighted the pore development during the microwave irradiation period. A similar phenomenon was also observed by Njoku et al., who reported the surface morphology of rambutan peel-based ACs having a series of uniform cavities around the surface due to activation by KOH [4].

Fig. 3 should be put here.

3.3.3 Functional groups analysis of ASAC

The surface chemistry of AS and ASAC was studied by FTIR spectroscopy in the infrared

spectral region of 4000–400 cm^{-1} (Fig. 4). AS contained much more bands than ASAC, with some major differences. The broad band at approximately 3450 cm^{-1} was observed for all samples, which was attributed to the O–H stretching vibration of the hydroxyl functional groups [13, 27]. The intense band at approximately 2950 cm^{-1} for AS was assigned to the C–H stretching vibration [28], which disappeared for ASAC, indicating the removal of hydrogen by activation. A band at approximately 2359 cm^{-1} for AS and ASAC was attributed to C≡C (alkynes), which was also reported similarly by Foo et al. [29]. A series of complex bands was detected in the range of 800–1630 cm^{-1} for AS, which was significantly reduced after activation. This phenomenon is possibly due to the breakdown of the chemical bonds in the raw material [30]. Compared with the bands located at 1630, 1390, 1255, 1085 and 800 in the spectra of the AS attributed to O-H bending vibrations, C-O-C (esters or phenol), C-O-C (ether) group, C-O stretching vibration and C-H blending or benzene, these bands in ASAC were weakened [5, 31]. The signal at 550 cm^{-1} was assigned to the C–O–H bending vibration [32].

Fig. 4 should be put here.

The compositional chemistry of surfaces of both AS and ASAC was analyzed by XPS, as shown in Fig. 5a. The observed spectra contained distinct peaks for C and O. The relative content of these elements was calculated and listed in Table 5. The percentage amounts of C, O, and S were: 72.07%, 26.88%, and 1.05% in AS and 86.57%, 13.43% and 0.00% in ASAC, respectively, thereby indicating a small increase in the C amount and a decrease in the O amount after activation procedure.

The high-resolution spectra of C 1*s* and O 1*s* were further analyzed by a curve-fitting

297 procedure, based on the Gaussian–Lorentzian function after baseline subtraction with
298 Shirley's method. Four components were considered to comprise the C 1*s* spectra [33] with
299 chemical shifts corresponding to: C–C (284.5 eV), C–O–R (285.8 eV), C=O (287.0 eV), and
300 COOR (289.2 eV). The fitting curves of these groups are illustrated in Fig. 5b-c, Fig. 5d-e
301 shows the deconvolution of the O 1*s* spectra for the AS and ASAC produced four peaks at
302 533.3, 534.2, 535.1, and 535.7 eV; these peaks represented O=C, O-C, R-O-C=O, and
303 C-OOH, respectively, and the relative content of each group is listed in Table 5. The results
304 suggest that the C–C group was predominant for the ASAC, which comprised close to 60% of
305 the carbon species. Moreover, relative contents of oxygen showed a significant decrease. For
306 oxygen species, the analysis suggested an increase in C=O group and a decrease in other
307 oxygen-groups for the ASAC (Fig. 5d-e). Liu et al. showed a similar phenomenon with the
308 reduction of oxygen-containing groups in AC, which is consistent with the FTIR and XPS
309 spectra [34].

310 **Fig. 5 should be put here.**

311 **3.4 Adsorption studies of MB**

312 **3.4.1 Effect of pH on the adsorption of MB onto ASAC**

313 The adsorption behavior of MB onto ASAC at different pH values was shown in Fig. 6.
314 The effect of pH was conducted by varying the pH of dye solutions from 2 to 12 with an
315 initial concentration of 500 mg/L, and the adsorption capacity showed an increase with the
316 increase of pH. Particularly, the adsorption capacity has a significant enhancement at pH of
317 6-8, which could be related to the protonation of MB in acidic medium, which triggers a
318 competitional effect between excessive amounts of H^+ and cationic dye on adsorption sites.

As the solution pH increases, ASAC may become more negatively charged and the formation of such electric double layer facilitates in changing the polarity, which lead into the enhancement of adsorption capacity. The effect of pH can be described on the basis of pH_{pzc}. The pH_{pzc} of ASAC was identified to be 6.16. When the solution pH < pH_{pzc}, activated carbon adsorbent will react as a positive surface, but when the solution pH > $pH_{pzc,}$ it will act as a negative surface. Therefore, for pH values above 6.16, the formation of electric double layer changes its polarity, which causes an increase in the surface charge density and electrostatic force of attraction. It unveils the dual adsorption of MB onto ASAC i.e. Physical adsorption as well as chemical adsorption, and the mechanism of chemical adsorption include the reaction between hydroxyl and carbonyl functional groups on the surface of the ASAC and MB. Positive charge on MB and OH^- on ASAC react according to the following reaction:

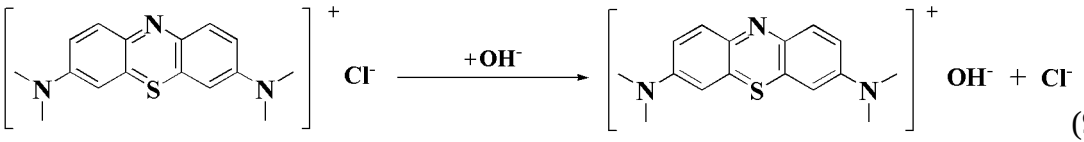

(9).

Fig. 6 should be put here.

3.4.2 Adsorption kinetics

The experimental data obtained for the AC from the initial concentrations of MB solution (300 and 500 mg/L) were fitted to the pseudo-first-order and pseudo-second-order models (Fig. 7). Rapid adsorption occurred in the first 15 minutes and reached the equilibrium after 30 min, which indicates the favorable interaction between the adsorbent and adsorbate (Table 6). The data indicate that the adsorption of MB onto ASAC was best described by the pseudo-second-order model, which R^2 = 0.999, similar values of q_e were calculated and experimentally determined. These findings suggest that the MB–ASAC system followed the

pseudo-second-order model, and the overall rate of adsorption process was controlled by physisorption at the beginning of adsorption and chemisorption after the first stage, which has already been explained by the effect of pH on the adsorption of MB onto ASAC. The same behavior was also observed by Foo et al. [29].

Fig. 7 should be put here.

3.4.3 Adsorption isotherms

The plots of the nonlinear Langmuir and Freundlich isotherm models for the adsorption of MB onto ASAC at 20 °C in line with Eq. (6) and (7) are presented in Fig. 8. The isotherm parameters determined from the slopes, as well as with the correlation coefficients of the isotherm models are summarized in Table 7. The equilibrium data were valid for the Langmuir isotherm model (R_{adj}^2 = 0.989), demonstrating the adsorption of MB onto ASAC from aqueous solutions by a monolayer formation. This result was in conformity with the previous result of nitrogen adsorption-desorption authenticating the monolayer adsorption phenomenon. The present results are quite consistent with previous researches on the adsorption of MB onto ACs prepared from pomelo skin and oil palm (*Elaeis*) empty fruit bunch by microwave-assisted chemical activation [32, 35].

Fig. 8 should be put here.

4. Conclusions

This study proposes a remarkable adsorbent ASAC through microwave heating method from the agricultural waste of AS. RSM was successfully used to optimize the conditions for ASAC preparation. The optimal activation conditions are as follows: a mass ratio ($ZnCl_2$/AS) of 3:1 (w/w), a microwave heating time of 15 min, and a microwave power of 900 W. The

resulting BET surface area of ASAC was 839.60 m^2/g, and the total pore volume was 0.406 cm^3/g. The yield and MB adsorption of ASAC under optimum conditions were 39.67% and 314.20 mg/g, respectively. These results indicated that the mass ratio and microwave power were the significant factors that affected carbon yield and MB adsorption. All statistical tools proved the excellent operational efficiency of ASAC. The adsorption behavior could be favorably described by the pseudo-second-order models and Langmuir isotherm. The excellent adsorption capacity of ASAC against MB validated its supremacy over the so far reported absorbents. Thus, the short microwave heating time and simplicity of the process demonstrated that microwave-assisted activation is a promising method for converting the AS into an excellent adsorbent, which could be employed in the remediation of aquatic environment as well as in chemical industry.

Acknowledgments

This work was supported financially by funding from the National Natural Science Foundation of China (51262025) and International scientific and technological cooperation project of Xinjiang Bingtuan (2013BC002).

References

[1] Walker GM, Weatherley LR. Sep. Sci. Technol. 2000, 35, 29-1341.

[2] Hesas RH, Arami-Niya A, Daud WMAW, Sahu JN. Chem. Eng. Res. Des. 2013, 91, 2447-2456.

[3] Tan IAW, Ahmad AL, Hameed BH. Chem. Eng. J. 2008, 137, 462-470.

[4] Njoku VO, Foo KY, Asif M, Hameed BH. Chem. Eng. J. 2014, 250, 198-204.

[5] Xiao H, Peng H, Deng SH, Yang XY, Zhang YZ, Li YW. Bioresour. Technol. 2012, 111, 127-133.

[6] Saka C. J. Anal. Appl. Pyrol. 2012, 95, 21-24.

[7] Wang X, Liang X, Wang Y, Wang X, Liu M, Yin D, Xia S, Zhao J, Zhang Y. Desalination 2011, 278, 231-237.

[8] Achawa OW and Afraneb G. Micropor. Mesopor. Mat. 2008, 112, 284-290.

[9] Ozhan A, Sahin O, Saka C, Kucuk MM. Cellulose. 2014, 21, 2457-2467

[10] J. Pezoti junior O, Cazetta AL, Gomes RC, Barizao EO, Souza IPAF, Martins AC, Asefa T, Almeida VC. Anal. App. Pyrol. 2014, 105, 166-176.

[11] Xiao XM, Tian F, Yan YJ, Wu ZS. J. Shihezi Univ. 2014, 4, 485-490.

[12] Xiao XM, Tian F, Yan YJ, Wu ZS, Wu ZL, Cravotto G. Korean J. Chem. Eng. 2015, 32, 1129-1136..

[13] Sahu JN, Acharya J, Meikap BC. Bioresour. Technol. 2010, 101, 1974-1982.

[14] Guses A, Dogar C, Yalcin M, Acikyildiz M, Bayrak R, Karaca S. J. Hazard. Mater. 2006, 131, 217-228.

[15] Al-Ghouti MA, Khraisheh MAM, Ahmad MNM, Allen S. J. Hazard. Mater. 2009, 165,

589-598.

[16] Ge XY, Tian F, Wu ZL, Yan YJ, Cravotto G, Wu ZS. Chem. Eng. Process. 2015, 91, 67-77.

[17] Freundlich H. Z. Phys. Chem. 1906, 57, 384-470.

[18] Zhong ZY, Yang Q, Li XM, Luo K, Liu Y, Zeng GM. Ind. Crop. Prod. 2012, 37, 178-185.

[19] Basta AH, Fierro V, El-Saied H, Celzard A. Bioresour. Technol. 2009, 100, 3941-3947.

[20] Duan XH, Srinivasakannan C, Peng JH, Zhang LB, Zhang ZY. Fuel Process Technol. 2011, 92, 394-400.

[21] Brum SS, Bianch ML, Silva VL, Goncalves M, Guerreiro MC, Oliveira LCA. Quim. Nova 2008, 31, 1048-1052.

[22] Deng H, Yang L, Tao GH, Dai JL. J. Hazard. Mater. 2009, 166, 1514-152.

[23] Foo KY, Hameed BH. Bioresour. Technol. 2012, 111, 425-432.

[24] Kruk M, Jaroniec M. Chem. Mater. 2001, 13, 3169-3183.

[25] Foo KY, Hameed BH. Biomass Bioenerg. 2011, 35, 3257-3261.

[26] Foo KY, Hameed BH. Bioresour. Technol. 2011, 102, 9814-9817.

[27] Ge XY, Ma XF, Wu ZS, Xiao XM, Yan YJ. Res. Chem. Intermediat. 2015, 41, 7327-7347.

[28] Foo KY, Lee LK, Hameed BH. Chem. Eng. J. 2013, 223, 604-610.

[29] Foo KY, Hameed BH. Chem. Eng. J. 2012, 180, 66-74.

[30] Yagmur E. J. Porous Mat. 2012, 19, 995-1002.

[31] Silverstein, RM, Webster, FX, Kiemle, DJ, Spectrometric Identification of Organic Compounds, 7th ed., John Wiley and Sons, New York, 2006.

[32] Foo KY, Hameed BH. Chem. Eng. J. 2011, 173, 385-390.

[33] Ryu Z, Rong H, Zheng J, Wang M, Zhang B. Carbon 2002, 40, 1131-1150.

[34] Liu QS, Zheng T, Wang P, Guo L. Ind. Crops Prod. 2010, 31, 233-238.

[35] Foo KY, Hameed BH. Desalination 2011, 275, 302-305.

Table captions

Table 1 Factorial design matrix and experimental response values.

Table 2 Analysis of variance for response surface quadratic model for adsorption capacity of MB.

Table 3 Comparison of adsorption capacities of various adsorbents for MB.

Table 4 Surface physical characteristics of the ASAC and other ACs.

Table 5 Relative contents of various elements and peak parameters of different C 1*s* and O 1*s* components of AS and ASAC samples based on the XPS spectra.

Table 6 Pseudo-first-order and pseudo-second-order kinetic rate constants for the adsorption of MB onto ASAC at 20 °C.

Table 7 Isotherm model parameters for the adsorption of MB onto ASAC at 20 °C.

439 **Table 1**

Std	Run	Mass ratio X_1(w/w)	Microwave heating time X_2(min)	Microwave power X_3(W)	Y_1(mg/g)	Y_2 (%)
3	1	1:1	20	700	179.80	36.00
11	2	2:1	10	900	209.81	34.70
1	3	1:1	10	700	164.83	35.50
7	4	1:1	15	900	194.73	37.00
6	5	3:1	15	500	239.59	40.00
12	6	2:1	20	900	194.81	36.00
8	7	3:1	15	900	314.20	39.67
2	8	3:1	10	700	239.55	34.00
5	9	1:1	15	500	164.82	38.50
10	10	2:1	20	500	194.86	31.00
4	11	3:1	20	700	269.32	39.00
9	12	2:1	10	500	164.92	49.70
16	13	2:1	15	700	224.64	38.70
13	14	2:1	15	700	209.56	42.00
14	15	2:1	15	700	179.79	45.00
17	16	2:1	15	700	194.74	38.70
15	17	2:1	15	700	209.83	63.30

440

441 **Table 2**

Source	Sum of squares	DF	Mean square	F-Value	Prob. > F
Model	23349.22	9	2594.36	9.92	0.0032
X_1	16063.49	1	16063.49	61.41	0.0001
X_2	445.21	1	445.21	1.70	0.2333
X_3	2788.55	1	2788.55	10.66	0.0138
X_1X_2	54.76	1	54.76	0.21	0.6611
X_1X_3	499.52	1	499.52	1.91	0.2095
X_2X_3	504.90	1	504.90	1.93	0.2073
X_1^2	2315.18	1	2315.18	8.85	0.0207
X_2^2	800.23	1	800.23	3.06	0.1238
X_3^2	5.80	1	5.80	0.022	0.8858
Residual	1831.09	7	261.58		
Lack of fit	668.72	3	222.91	0.77	0.562
Pure error	1162.37	4	290.59		
Cor total	25180.31	16			

442

443

444 **Table 3**

Precursors of ACs	Mass of AC (g)	Initial concentrations of MB (mg/L)	Volume of MB (mL)	pH	Adsorption capacity of MB (mg/g)	References
Macadamia nut endocarp	0.025	500	25	-	194.7	[11]
Coffee waste	0.1	1000	10	5.3	188.7	[22]
Cotton stalk	0.1	1500	25	-	193.5	[23]
Wood sawdust	0.2	500	200	-	425.3	[24]
Almond shell	0.1	1500	50	6.16	314.2	This work

445

446

447 **Table 4**

Precursors of ACs	S_{BET} (m^2/g)	Micropore area (m^2/g)	V_T (cm^3/g)	Micropore Volume (cm^3/g)	Average pore width (nm)	References
Almond shell	839.60	383.64	0.406	0.152	0.83	This work
Pistachio shell	700.53	-	0.375	-	2.14	[25]
Rice husk	752	346	0.64	0.26	3.41	[26]
Cotton stalk	794.84	156.69	0.63	0.083	3.20	[23]

448

449

Table 5

	Relative content (%)			Relative content (%) of C 1*s*				Relative content (%) of O 1*s*			
	C	O	S	C-C	C-O-R	C=O	C-OOR	C=O	C-O	C-OOR	C-OOH
AS	72.07	26.88	1.0	13.15	41.97	25.59	19.29	22.55	32.73	24.05	20.67
ASAC	86.57	13.43	0.0	59.18	22.18	11.47	7.17	39.17	26.21	17.18	17.44

Table 6

C_0(mg/L)	$q_{e,exp}$(mg/g)	Pseudo-first-order			Pseudo-second-order		
		K_1(mg/g)	q_e(mg/g)	R^2	K_2(g/mg)	q_e(mg/g)	R^2
300	148.59	0.770	148.45	0.785	0.050	149.25	0.999
500	249.56	0.508	248.51	0.842	0.160	250.00	0.999

Table 7

Isotherms	Langmuir			Freundlich		
Constants	q_m (mg/g)	K_L (L/mg)	R^2	n	K_F (mg/g)(L/mg)$^{1/n}$	R^2
	500.00	0.307	0.989	2.22	112.449	0.717

Figure captions

Fig. 1 Three-dimensional graphic of response surface for response: mass ratio and activation time (a), mass ratio and microwave power (b), activation time and microwave power (c).

Fig. 2 N_2 adsorption and desorption isotherms at 77K (a) and pore size distribution (b) of ASAC.

Fig. 3 SEM images of AS (a), and ASAC (b).

Fig. 4 FTIR spectra of AS and ASAC.

Fig. 5 XPS survey spectra and high-resolution spectra of AS and ASAC: (a) survey scans; (b) AS: C 1*s*; (c) ASAC: C 1*s*; (d) AS: O 1*s*; (e) ASAC: O 1*s*.

Fig. 6 Effect of pH on the adsorption of MB onto ASAC at 20 °C (C_0 = 500 mg/L, contact time = 30 min, activated carbon mass = 0.1 g)

Fig. 7 Effect of time on the adsorption of MB onto ASAC at 20 °C (pH = 6.16, 0.1 g of ASAC).

Fig. 8 Plots of Langmuir and Freundlich models for adsorption of MB onto ASAC (pH = 6.16, contact time = 30 min, 0.1 g of ASAC).

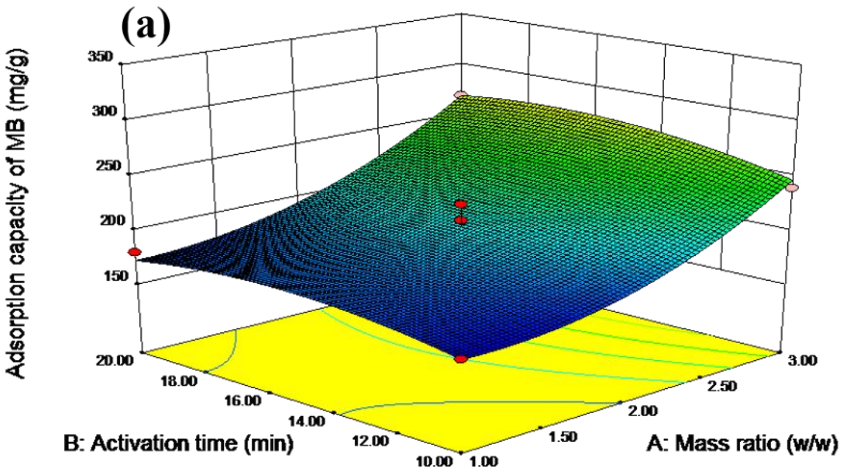

485

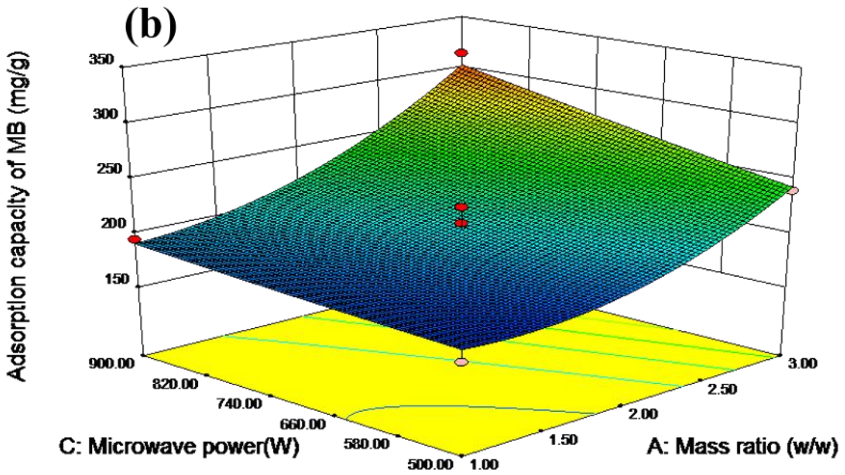

486

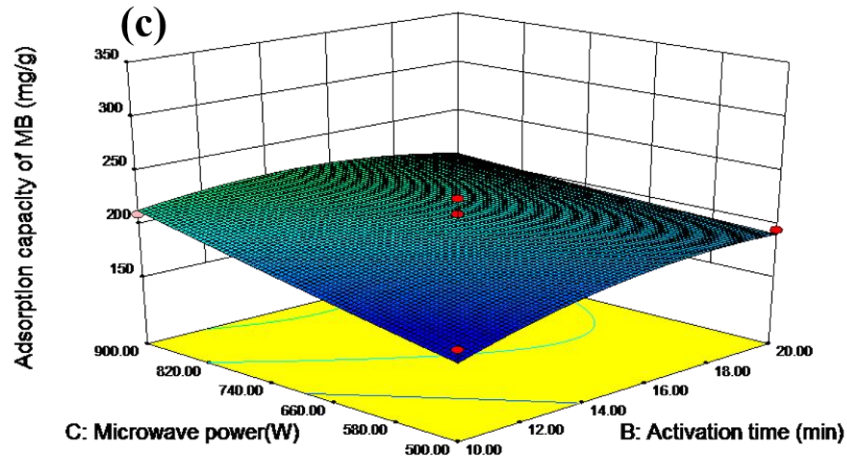

487

488 **Fig. 1** Three-dimensional graphic of response surface for response: mass ratio and activation
489 time (a), mass ratio and microwave power (b), activation time and microwave power (c).

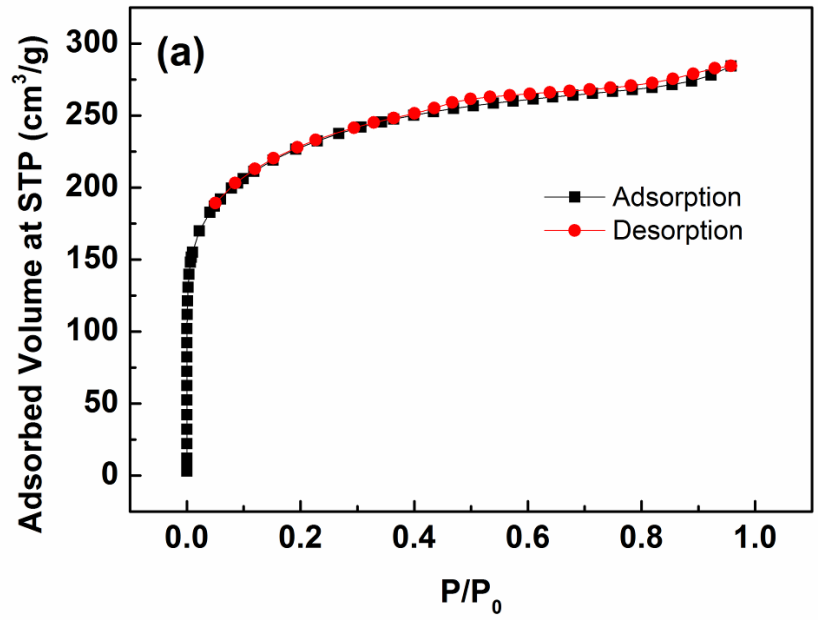

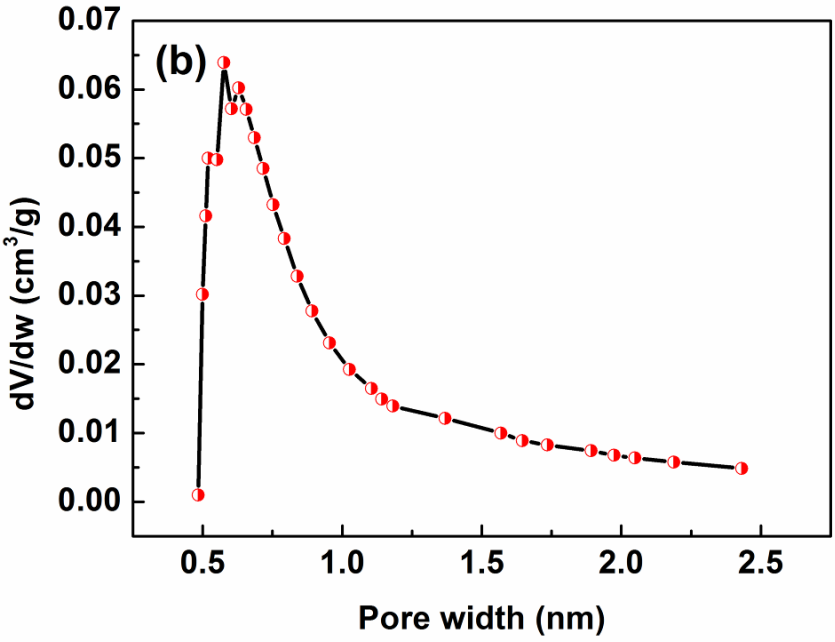

Fig. 2 N_2 adsorption and desorption isotherms at 77K (a) and pore size distribution (b) of ASAC.

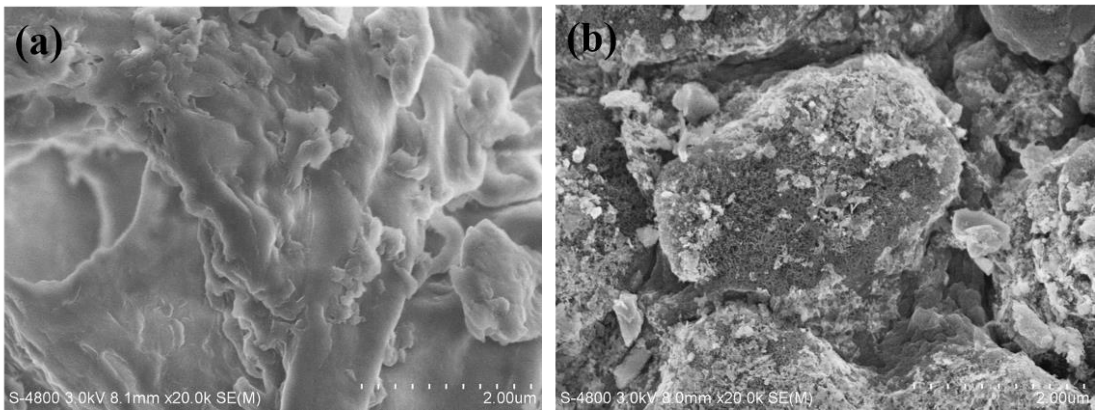

Fig. 3 SEM images of AS (a), and ASAC (b).

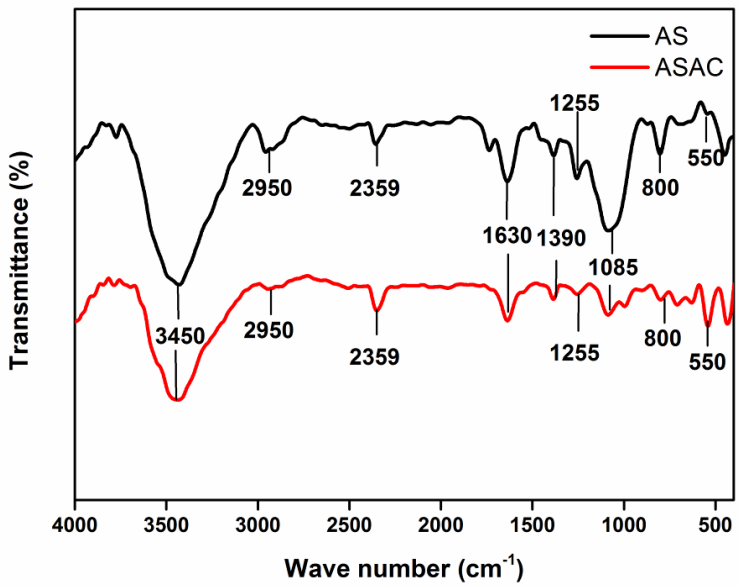

Fig. 4 FTIR spectra of AS and ASAC.

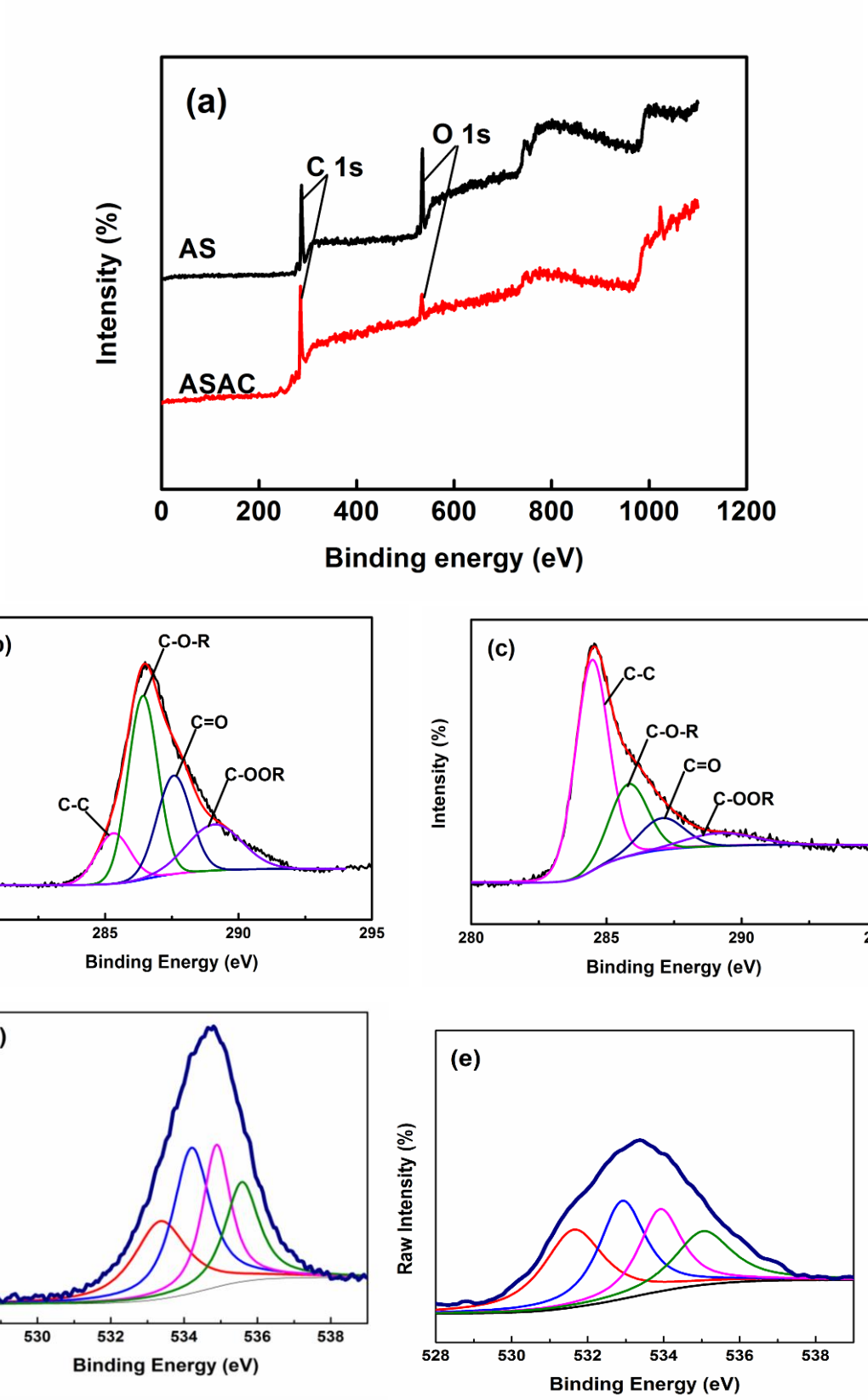

Fig. 5 XPS survey spectra and high-resolution spectra of AS and ASAC: (a) survey scans; (b) AS: C 1*s*; (c) ASAC: C 1*s*; (d) AS: O 1*s*; (e) ASAC: O 1*s*.

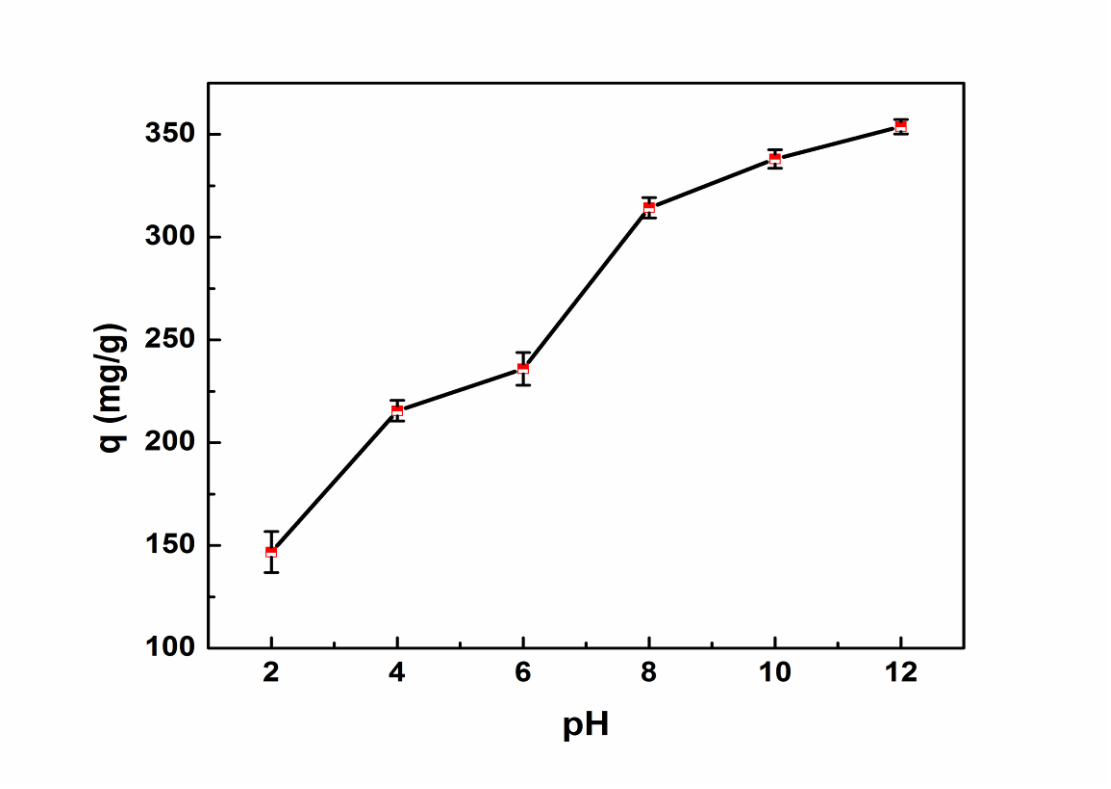

Fig. 6 Effect of pH on the adsorption of MB onto ASAC at 20 °C (C_0 = 500 mg/L, contact time = 30 min, activated carbon mass = 0.1 g)

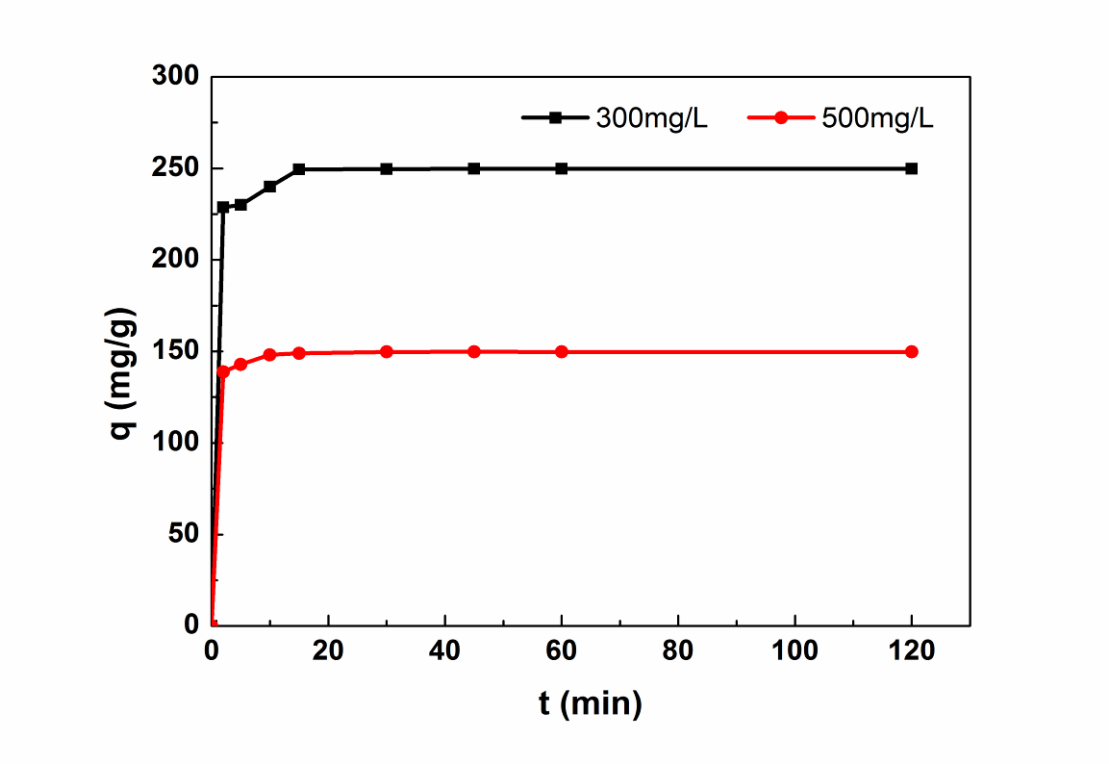

Fig. 7 Effect of time on the adsorption of MB onto ASAC at 20 °C (pH = 6.16, 0.1 g of ASAC).

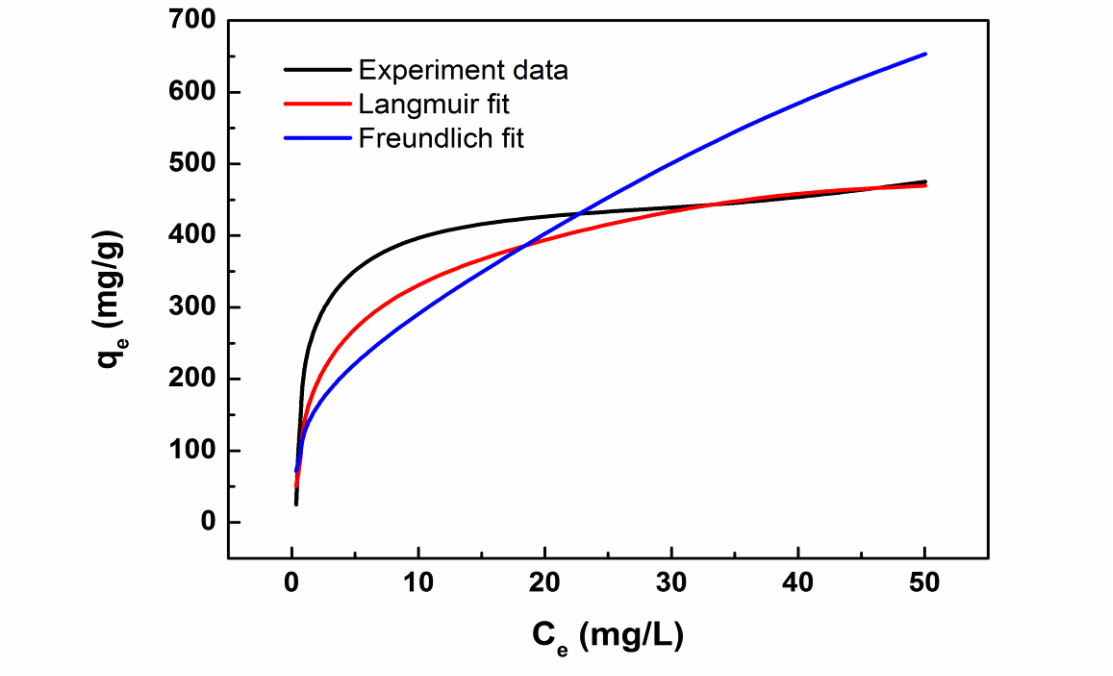

Fig. 8 Plots of Langmuir and Freundlich models for adsorption of MB onto ASAC (pH = 6.16, contact time = 30 min, 0.1 g of ASAC).

528 **Graphical abstract figure**

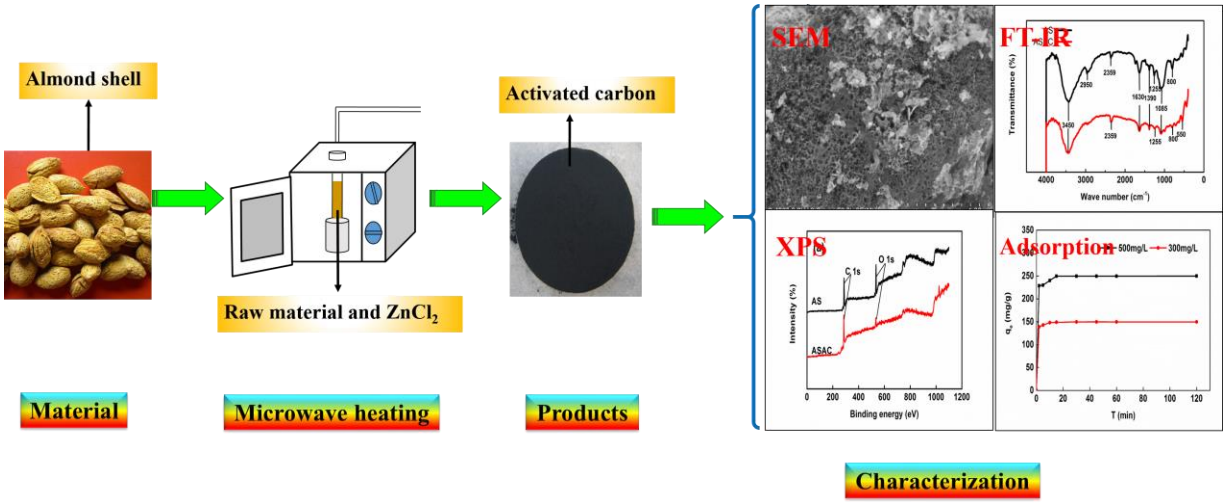

529